REPORT DOCUMENTATION PAGE

1. REPORT DATE (DD-MM-YYYY)	2. REPORT TYPE	3. DATES COVERED (From - To)
10-02-2012	Conference Proceeding	

4. TITLE AND SUBTITLE	5a. CONTRACT NUMBER
Automated Detection and Removal of Cloud Shadows on HICO Images	
	5b. GRANT NUMBER
	5c. PROGRAM ELEMENT NUMBER
	0602435N

6. AUTHOR(S)	5d. PROJECT NUMBER
Ruhul Amin, Richard Gould, Weilin Hou, ZhongPing Lee, Robert Arnone	
	5e. TASK NUMBER
	5f. WORK UNIT NUMBER
	73-6287-A1-5

7. PERFORMING ORGANIZATION NAME(S) AND ADDRESS(ES)	B. PERFORMING ORGANIZATION REPORT NUMBER
Naval Research Laboratory Oceanography Division Stennis Space Center, MS 39529-5004	NRL/PP/7330-11-0686

9. SPONSORING/MONITORING AGENCY NAME(S) AND ADDRESS(ES)	10. SPONSOR/MONITOR'S ACRONYM(S)
Office of Naval Research One Liberty Center 875 North Randolph Street, Suite 1425 Arlington, VA 22203-1995	ONR
	11. SPONSOR/MONITOR'S REPORT NUMBER(S)

12. DISTRIBUTION/AVAILABILITY STATEMENT

Approved for public release, distribution is unlimited.

20120217368

13. SUPPLEMENTARY NOTES

14. ABSTRACT

Clouds cause a serious problem for optical satellite sensors. Clouds not only conceal the ground, they also cast shadows, which cause either a reduction or total loss of information in an image, by reducing the illumination falling on the shadowed pixels. Ocean color bio-optical inversion algorithms rely on measurements of remote sensing reflectance ((λ) rs R) at each pixel. If shadows are not removed properly across a scene, erroneous (λ) rs R values will be calculated for the shadowed pixels, leading to incorrect retrievals of ocean color products such as chlorophyll. The cloud shadow issue becomes significant especially for high-resolution sensors such as the Hyperspectral Imager for the Coastal Ocean (HICO). On the other hand, the contrast of pixels in and outside a shadow provides opportunities to remove atmospheric contributions for ocean color remote sensing. Although identifying cloud is relatively straightforward using simple brightness thresholds, identifying their shadows especially over water is quite challenging because the brightness of the shadows is very close to the brightness of neighboring sunny regions especially in deep waters. In this study, we present automated procedures for our recently proposed cloud shadow detection technique called the Cloud Shadow Algorithm (CSA) and Lee et al. (2007) cloud and shadow atmospheric correction algorithm. We apply both automated procedures to HICO imagery and show examples of the results.

15. SUBJECT TERMS

atmospheric correction, HICO, cloud shadow, optical algorithm, automated, ocean color, remote sensing

16. SECURITY CLASSIFICATION OF:			17. LIMITATION OF ABSTRACT	1B. NUMBER OF PAGES	19a. NAME OF RESPONSIBLE PERSON
a. REPORT	b. ABSTRACT	c. THIS PAGE	UU	10	Richard Gould
Unclassified	Unclassified	Unclassified			19b. TELEPHONE NUMBER (Include area code) 228-688-5587

Automated Detection and Removal of Cloud Shadows on HICO Images

Ruhul Amin*[a], Richard Gould[a], Weilin Hou[a], Zhongping Lee[b] and Robert Arnone[a]

[a]Naval Research Laboratory, Code 7333, Stennis Space Center, Mississippi 39529, USA;
[b]GRI, Mississippi State University, Stennis Space Center, MS 39529, USA

ABSTRACT

Clouds cause a serious problem for optical satellite sensors. Clouds not only conceal the ground, they also cast shadows, which cause either a reduction or total loss of information in an image, by reducing the illumination falling on the shadowed pixels. Ocean color bio-optical inversion algorithms rely on measurements of remote sensing reflectance ($R_{rs}(\lambda)$) at each pixel. If shadows are not removed properly across a scene, erroneous $R_{rs}(\lambda)$ values will be calculated for the shadowed pixels, leading to incorrect retrievals of ocean color products such as chlorophyll. The cloud shadow issue becomes significant especially for high-resolution sensors such as the Hyperspectral Imager for the Coastal Ocean (HICO). On the other hand, the contrast of pixels in and outside a shadow provides opportunities to remove atmospheric contributions for ocean color remote sensing. Although identifying cloud is relatively straightforward using simple brightness thresholds, identifying their shadows especially over water is quite challenging because the brightness of the shadows is very close to the brightness of neighboring sunny regions especially in deep waters. In this study, we present automated procedures for our recently proposed cloud shadow detection technique called the Cloud Shadow Algorithm (CSA) and Lee et al. (2007) cloud and shadow atmospheric correction algorithm. We apply both automated procedures to HICO imagery and show examples of the results.

Keywords: atmospheric correction, HICO, cloud shadow, optical algorithm, automated, ocean color, remote sensing

1. INTRODUCTION

Hyperspectral information collected by optical satellite sensors can provide important information for various global remote sensing applications. However, clouds cause a serious problem for these sensors, especially over humid tropical regions. Throughout the year about 2/3 of the Earth's surface is always covered by the clouds (Belward and Valenzuela, 1991). The problem for the optical sensor is that clouds not only conceal the ground but they also cast shadows and these shadows also occur in the observed images along with the clouds. Unlike airborne imaging where shadows can be minimized by flying at certain times during the day, low Earth orbit satellite-based sensors are limited to acquiring images at fixed times of the day. If the solar elevation is low at the time, then the presence of shadow will be unavoidable. The main problem caused by shadows is either a reduction or total loss of information in an image (Dare, 2005). Since ocean color algorithms are developed for water pixels illuminated by both direct solar irradiance and sky light, the radiance values in shadow pixels leads to the corruption of biophysical parameters derived at those pixels. Cloud shadow can produce errors of 30-40% in the observed reflectance from the affected pixels over lands (Simpson and Stitt, 1998). Similar errors can be expected over waters as well although such studies have never been conducted. Since ocean color products are retrieved based on the assumption that the remote sensing reflectances are accurate, a small inaccuracy in the reflectance can lead to significant errors in the retrieved products. Particularly, since most of the

*ruhul.amin@nrlssc.navy.mil; phone 228 688-5000

product retrieval algorithms are band ratio algorithms, a small disproportionate alteration in the spectral reflectance amplitude can changes the band ratios considerably hence the retrieved products (Amin et al., 2009; Amin et al. 2008). On the other hand, cloud shadow detection in ocean color scene can be important and beneficial, since cloud shadowed pixels in combination with pixels in a neighboring sunny region of similar optical properties can be used to remove atmospheric effects from these scenes (Carder et al., 1992; Lee et al., 2007; Reinersman et al., 1998). These neighboring sunny pixels can then be used as known reflectance targets for validation of the sensor calibration and atmospheric corrections (Carder et al., 1992; Reinersman et al., 1998).

There are numerous algorithms for cloud detection (Khlopenkov and Trishchenko, 2007; Ackerman et al., 1998; Cihlar and Howarth, 1994; Rossow and Garder, 1993). However, relatively few cloud shadow detection algorithms (Simpson and Stitt, 1998; Chen et al., 2002; Wang and Ono, 1999; Simpson et al., 2000) has appeared in the literature even though accurate detection of cloud shadow is important for many atmospheric and terrestrial applications. Most of the shadow detection algorithms described in the literature deals with shadows over land. Few studies specifically on shadow detection over water have been conducted, while shadow detection over water is becoming significant as the spatial resolutions of the ocean color sensors are getting finer. This is because the small scale shadow features appear in the acquired images.

The fundamental measurement in ocean color remote sensing is the water-leaving radiance, the upwelling spectral distribution of the radiance from the ocean. Geophysical parameters such as chlorophyll can be retrieved from this water-leaving signal since it contains information about the optically-active components in the water column. However, only about 10% of the total signal measured by the ocean color sensors contains information about the waters; the rest represents scattering from aerosols and air molecules. The goal of the atmospheric correction over the ocean is to remove contributions from the atmosphere and reflection from the sea surface.

Gordon and Wang (1994) developed an atmospheric correction scheme for the open ocean where the aerosol contribution is estimated using Top of the Atmosphere (TOA) radiance/reflectance signals obtained from near infrared (NIR) bands. This approach assumes that the ocean is optically black in the NIR bands due to the strong water absorption. Although this technique works well in the open ocean, it breaks down in optically complex coastal waters since the black pixel approximation no longer holds true due to strong reflections from organic and inorganic particulate matters. If water-leaving radiance is not negligible in the NIR bands then the retrieved aerosol loading will be overestimated, resulting in underestimated or even negative water-leaving radiances. The NIR-iterative procedure for the coastal waters (Stumpf et al., 2003) can be somewhat helpful in such situation reducing number of pixels with negative readings in the coastal waters. More recently, another atmospheric correction approach for coastal water was proposed (Wang and Shi, 2005) which uses short wave infrared (SWIR) bands. This approach is based on the fact that ocean water absorbs strongly in this spectral region, and the contributions of the in-water constituents are negligible and can safely be considered dark. However, HICO does not have these SWIR channels. Furthermore, the atmospheric reflectance itself is significantly weaker in SWIR region and spectral features are particularly difficult to resolve. In such situations, the cloud and shadow (C&S) atmospheric corrections (Lee et al., 2007; Reinersman et al., 1998) can be very helpful. However, C&S approach is limited to images with cloud and shadow present.

In this paper we present an automated procedure of our recently proposed cloud shadow detection technique called the Cloud Shadow Algorithm (CSA) (Amin et al., 2011). Furthermore, we present an automated procedure for the C&S atmospheric corrections (Lee et al., 2007) and test it on HICO data.

2. BACKGROUND OF THE CLOUD SHADOW DETECTION ALGORITHM

It can be easy to identify the cloud regions simply by using brightness thresholds, but it is difficult to identify the shadow regions this way because their brightness values can be very close to those of their neighbors or some other regions. Distinguishing shadows over water bodies based on spectral reflectance shape and amplitude information is also very difficult or possibly even impossible (Richter and Muller, 2005). Shadows over water pixels do not have any specific spectral features while the brightness varies with atmospheric conditions and imaging geometry. Therefore, the brightness or the spectral shape alone may not be appropriate for shadow detection. However, brightness values from shadow and close by sunny regions over water can provide a great deal of information if a small portion of the image

(where optical properties of water and atmosphere is uniform) is examined at a time. This is because the water-leaving radiance over sunny pixels results from both direct and diffuse solar irradiance, while the water-leaving radiance over shadow pixels results from only diffuse solar irradiance. The path radiance from the shadow pixel to the sensor is also slightly lower depending on how much of the atmospheric path radiance is shadowed. Therefore, the total radiance at the TOA measured over the shadow pixels is slightly lower compare to the adjacent sunny pixels. Assuming the optical properties of water and atmosphere is homogeneous around shadow and adjacent sunny regions, examining the radiance difference amongst these small uniform regions together enables us to separate the shadow regions.

Although spectral radiance amplitude of shadow region is slightly lower than the neighboring sunny region, this difference is relatively small (Amin et al., 2011). Furthermore, because of different path radiance and water-leaving radiance, the measured radiance from some other sunny region may have exact same or sometimes even lower radiance than the shadow spectra (Amin et al., 2011 (see Fig. 1(c))). Therefore, the spectral shape or amplitude alone is not adequate enough to separate the two regions. However, to make them separable, the small differences in the spectral amplitudes particularly in blue-green regions can be amplified by integrating the spectra. The first part of our cloud shadow detection algorithm is to integrate the spectra which we called the Integrated Value (IV) and we define it as

$$IV = \int_{400nm}^{600nm} Lt(\lambda)d\lambda. \tag{1}$$

The IV index allows visual separation of the two regions to an observer. However, IV itself is not adequate to separate based on a threshold. This is because the IV index from a shadow region can be very close to, or even higher than, the IV index of some other sunny regions (Amin et al., 2011).

To separate the shadow and sunny pixels using a constant threshold, we normalize the IV index of the pixel under investigation, by the mean of the IV indices within a spatial Adaptive Sliding Box (ASB) centered on this pixel. The selection of ASB size is explained after Eq. 2.

Based on the optical characteristics of the water and atmosphere in the shadow and neighboring sunny region, our cloud shadow detection technique called the Cloud Shadow Algorithm (CSA) is defined as:

$$CSA = \frac{IV_c}{\langle IV_{ASB}\rangle}, \tag{2}$$

where IV_c represents the IV index of the pixel (the central pixel of the ASB) which needs to be classified as a shadow or sunny pixel. The $\langle IV_{ASB}\rangle$ represents the spatial mean of IV indices within the selected ASB of this pixel. This process should be repeated for all pixels that need to be classified as shadow or sunny. Note that before applying the CSA, clouds needs to be removed properly or spurious results can be expected. Additionally, the CSA might break down in turbid coastal waters since water or even the atmosphere may not be homogeneous within the ASB. Thus the CSA is mainly for deep waters, where atmospheric and marine optical properties can be assumed homogeneous within the ASB. The ASB needs to be selected carefully so that it only contains shadow and sunny pixels or only sunny pixels. If the ASB contains only sunny pixels and the pixel under examination is also sunny, the CSA value for this pixel would be around one since the mean of the ASB and IV index would be about the same. While if the ASB contains both shadow and sunny pixels and the pixel under examinations is sunny, the CSA value will be greater than one since the mean of the ASB will be slightly lower than the IV index of the pixel under examination. On the other hand, if the pixel under examination happens to be shadowed, the CSA value would be less than one since the IV index of this shadow pixel would be smaller than the mean of the ASB. Now, if ASB contains only shadowed pixels, it can be problematic since the CSA value will be around one, like the case of only sunny pixels. They will be classified as sunny pixels if the CSA threshold is put less than one. That is why it is important to select the ASB in such a way so that it is bigger than the shadowed region. This can be achieved by using the cloud size information which is relatively easy to detect, even using simplistic brightness thresholds.

3. AUTOMATION AND RESULTS

3.1 Shadow Algorithm

The CSA cloud shadow algorithm is developed for homogeneous water bodies such as open waters. Fig. 1 shows the processing steps of the automated cloud shadow detection using the CSA approach. The first step of the shadow detection is to remove lands, clouds, and non-homogeneous water pixels from the acquired ocean color imageries. The input image should only have sunny and shadow pixels from homogeneous water bodies. The next step is to calculate the IV indices of the input pixels. Once the IV indices are calculated, the ASB is selected for each pixel and the CSA values are calculated. Then using the proposed CSA threshold (CSA<=0.96) (Amin et al., 2011), the shadowed pixels are separated from the sunny pixels. Examples of automated shadow detection using the CSA method (using a constant 128 × 128 ASB) are shown in Fig. 2. Left panel of Fig. 2 shows a HICO image acquired over Virgin Islands on December 20, 2009 (image size: 270 × 400 pixels) where Fig. 2(a) is the true color image, Fig. 2(b) is the corresponding IV image and Fig. 2(e) is the corresponding CSA image. Right panel of Fig. 2 is another HICO image acquired over Samoa Island on October 2, 2010 (image size: 260 × 260 pixels) where Fig. 2(d) is the true color image, Fig. 2(e) is the corresponding IV image, and Fig. 2(f) is the corresponding CSA image. The clouds are shown in white on both CSA and IV images, while the shadows are shown in red on the CSA images and in slightly cooler color compare to the neighboring sunny region on the IV images. The sunny regions are shown in blue on the CSA image, and in slightly warmer color compare to the adjacent shadow regions on the IV images. The true color, IV and the CSA images agrees reasonably well on Fig. 2. The cloud shadows are clearly seen in red structures adjacent to the white clouds on the CSA images. Also the shape of the cloud shadow especially for the isolated cloud closely follows that of the cloud as expected which reconfirms the potential of the CSA method.

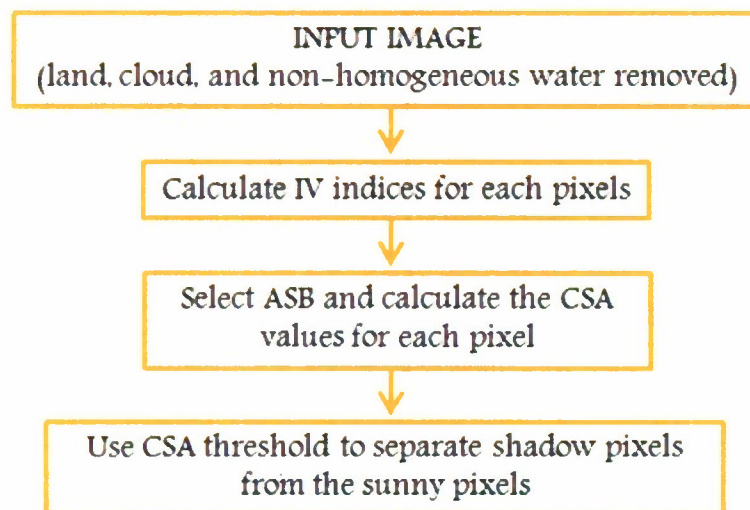## AUTOMATED CLOUD SHADOW DETECTION PROCEDURE

Figure 1. Processing steps of automated cloud shadow detection using the CSA method.
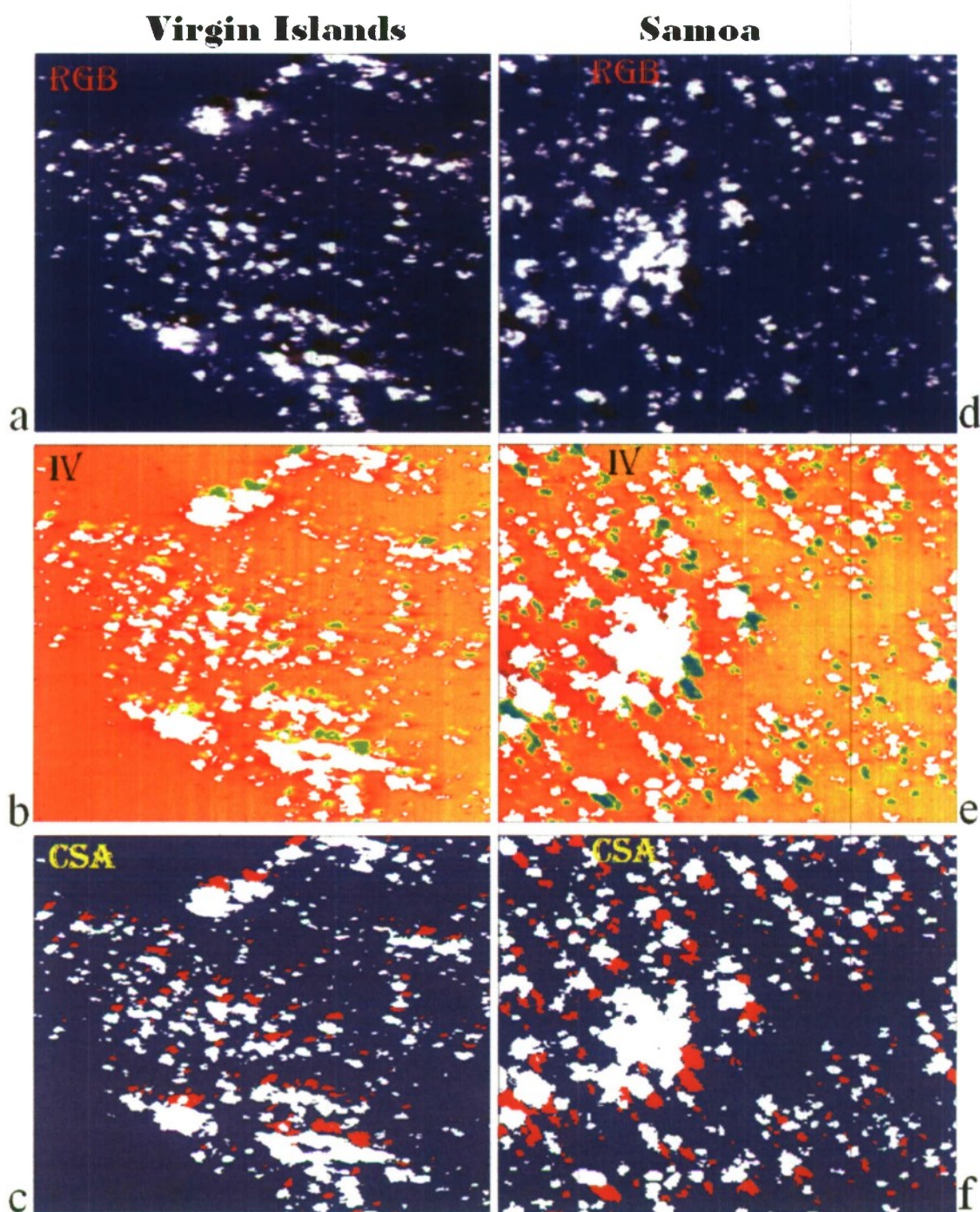
Figure 2. Examples of cloud shadow detection using the CSA method. Left panel: HICO image acquired over Virgin Islands on December 20, 2009 (image size: 270 × 400 pixels); (a) true color image, (b) corresponding IV image, and (c) corresponding CSA image. Right panel: HICO image acquired over Samoa on October 2, 2010 (image size: 260 × 260 pixels); (d) true color image, (e) corresponding IV image and (f) corresponding CSA image. The clouds are shown in white on both CSA and IV images, the shadows are shown in red on the CSA

images and in slightly cooler color on the IV image, and the sunny regions are shown in blue on the CSA image and in warmer color on the IV images. The true color, IV and the CSA images agrees pretty well. The Cloud shadows are clearly seen in red structures adjacent to the white clouds on the CSA images. The shape of the cloud shadow especially for the isolated cloud closely follows that of the cloud as expected. A 128 × 128 ASB was used to created the CSA images.

3.2 Atmospheric Correction Algorithm

The C&S atmospheric correction method (Lee et al., 2007; Reinersman et al., 1998) is appropriate for high-spatial resolution sensors such as HICO. This approach uses cloud and shadow pixels along with close by sunny pixels with similar optical properties. First, it estimates the atmospheric and sea-surface reflectance $L_a(\lambda)$ from a pair of adjacent pixels that are in and out of a cloud shadow while ignoring the slight (<5%) differences in the remote-sensing reflectance $R_{rs}(\lambda)$ under the two regions (Lee et al., 1998; Kirk, 1991; Morel and Gentili, 1993; Lee et al., 2004). Estimation of $L_a(\lambda)$ also requires an estimate of the ratio between the downwelling sky irradiance to total downwelling irradiance $E_d^{sky}(\lambda) / E_d(\lambda)$ which can be estimated using Radtran (Gregg and Carder, 1990) for a given location and time. The value of $E_d^{sky}(\lambda) / E_d(\lambda)$ depend on atmospheric conditions such as visibility, ozone depth, etc. However, since $E_d^{sky}(\lambda) / E_d(\lambda)$ is applied on the difference between $Lt_{sny}(\lambda)$ (total radiance measured over the sunny pixel) and $Lt_{sdw}(\lambda)$ (total radiance measured over the shadowed pixel), and this difference is significantly smaller than $Lt_{sny}(\lambda)$, errors in $E_d^{sky}(\lambda) / E_d(\lambda)$ have only very limited effects on $L_a(\lambda)$ estimation (Lee et al., 2007). Since the errors in $E_d^{sky}(\lambda) / E_d(\lambda)$ estimation have negligible effects (Lee et al., 2007), $E_d^{sky}(\lambda) / E_d(\lambda)$ were calculated with the default atmospheric parameters in Radtran. In order to calculate $R_{rs}(\lambda)$, the product of atmospheric transmittance and downwelling irradiance $t(\lambda)E_d(\lambda)$ just above the surface is also needed. For this component the total radiance over the cloud $Lt_{cld}(\lambda)$ is used to make the estimate which requires an estimation of remote-sensing reflectance (ρ) of observed clouds. The value of ρ was determined as recommended in (Lee et al., 2007) from a clear water pixel by assuming $R_{rs}(550nm) = 0.002 sr^{-1}$ (Gordon and Clark, 1981). Once the $R_{rs}(\lambda)$ is estimated to account for any residual contributions from the sky and sea surface, a spectrally constant value is removed from the calculated $R_{rs}(\lambda)$ in order to obtain an average of zero for the spectral range of 810-840 nm, where contributions from water are considered null (Mueller et al., 2002).

The processing steps of the automated C&S atmospheric corrections are shown in Fig. 3. The input image for the automated process should have land and non-homogeneous water pixels removed. The next step is to identify cloud, cloud shadow, and sunny pixels in the input image. We use a band ratio between the HICO band 35(548nm) and band 70(748nm) to separate the cloud pixels. After separating cloud pixels, we use the automated CSA cloud shadow detection approach (see Fig. 1) to separate the shadow and sunny pixels. Once cloud, cloud shadow, and sunny pixels are identified, we use blob detection to get cloud, could shadow, and sunny blobs. The cloud and cloud shadow blobs are narrowed down based on the blob size (keeping only blobs with 30 to 300 pixels). From these keeper blobs, we find the closest cloud and cloud shadow blobs based on the distance between the central pixels of each blobs. From the selected cloud and shadow blobs, we find the closest cloud and shadow pixels and take the $Lt_{cld}(\lambda)$ and $Lt_{sdw}(\lambda)$ respectively averaged over 3×3 pixels. Then from the selected shadow blob, we find the closest sunny pixel and take the

$Lt_{sny}(\lambda)$ averaged over 3×3 pixels. The $Lt_{sdw}(\lambda)$ and $Lt_{sny}(\lambda)$ along with the $E_d^{sky}(\lambda)\Big/E_d(\lambda)$ from Radtran are used to estimate the $L_a(\lambda)$. The ρ is estimated using the spectra from sunny pixel ($Lt_{sny}(\lambda)$) assuming the $R_{rs}(\lambda)$ is known (Lee et al., 2007). The $R_{rs}(\lambda)$ is then estimated for all the sunny pixels using the $L_a(\lambda)$, ρ and $Lt_{cld}(\lambda)$.

AUTOMATED CLOUD-SHADOW ATOMSPHERIC CORRECTIONS PROCEDURE

INPUT IMAGE
(land and non-homogeneous water removed)

↓

Identify cloud, shadow, and sunny pixels

↓

Select $Lt_{cld}(\lambda), Lt_{sdw}(\lambda)$ and $Lt_{sny}(\lambda)$ using blob detection

↓

Estimate $L_a(\lambda)$ using $Lt_{sdw}(\lambda)$ and $Lt_{sny}(\lambda)$

↓

Estimate $E_d^{sky}(\lambda)/E_d(\lambda)$ from RADTRAN for a given location at a given time

↓

Estimate cloud remote sensing reflectance (ρ)
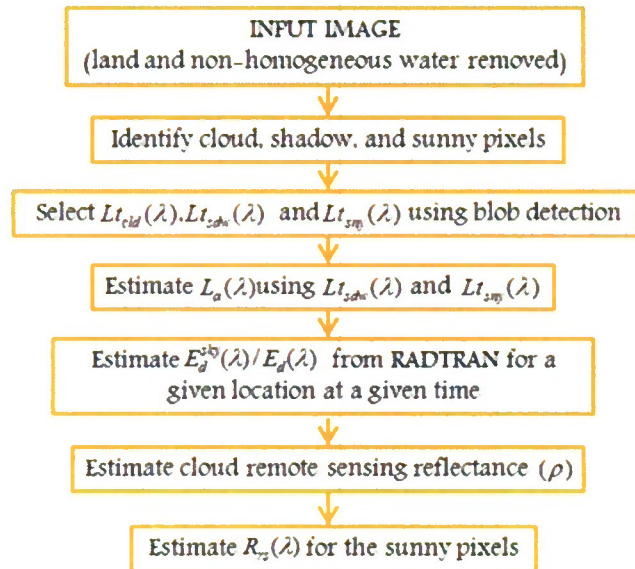
↓

Estimate $R_{rs}(\lambda)$ for the sunny pixels

Figure 3. Overview of the automated cloud and shadow atmospheric corrections process.

Fig. 4(a) shows the 1V image calculated from a HICO image acquired over Samoa Island on October 2, 2010 (image size: 380 × 380 pixels). The clouds are shown in white while the shadows are shown in slightly cooler color compare to the neighboring sunny regions. Since C&S atmospheric corrections requires spectra from a thick cloud and cloud shadow, we use additional conditions ($Lt_{cld}(548nm) > 5000(counts)$) and ($CSA <= 0.93$) to identify the thick clouds and thick cloud shadows respectively. The blue contours on Fig. 4(a) shows thick cloud blobs while the red contour shows the thick shadow blobs. The green circle with the arrows labeled with "cld", "sdw", and "sny" shows the automatically selected cloud, shadow, and sunny blobs respectively. The $Lt_{cld}(\lambda)$, $Lt_{sdw}(\lambda)$ and $Lt_{sny}(\lambda)$ (Fig. 4(b) solid spectra) are taken from these selected cloud, shadow, and sunny blobs respectively. The dashed spectra in Fig. 4(b) are selected manually from another far location (pixel locations: cld(91, 1622), sdw(99, 1631) and sny(104, 1620)) outside the portion (shown only 380 × 380 pixels of 512 × 2000 pixels) of the image shown in Fig. 4(a). The results ($R_{rs}(\lambda)$) from the automatically selected and manually selected pixels are show in Fig. 4(c) where blue $R_{rs}(\lambda)$ are the results of automated pixels selection while the red $R_{rs}(\lambda)$ are results of manual pixels selection. These $R_{rs}(\lambda)$ spectra are taken from the selected sunny blob labeled with "sny" in yellow (Fig. 4(a)). The agreement between the manually and automatically retrieved $R_{rs}(\lambda)$ is very reasonable.
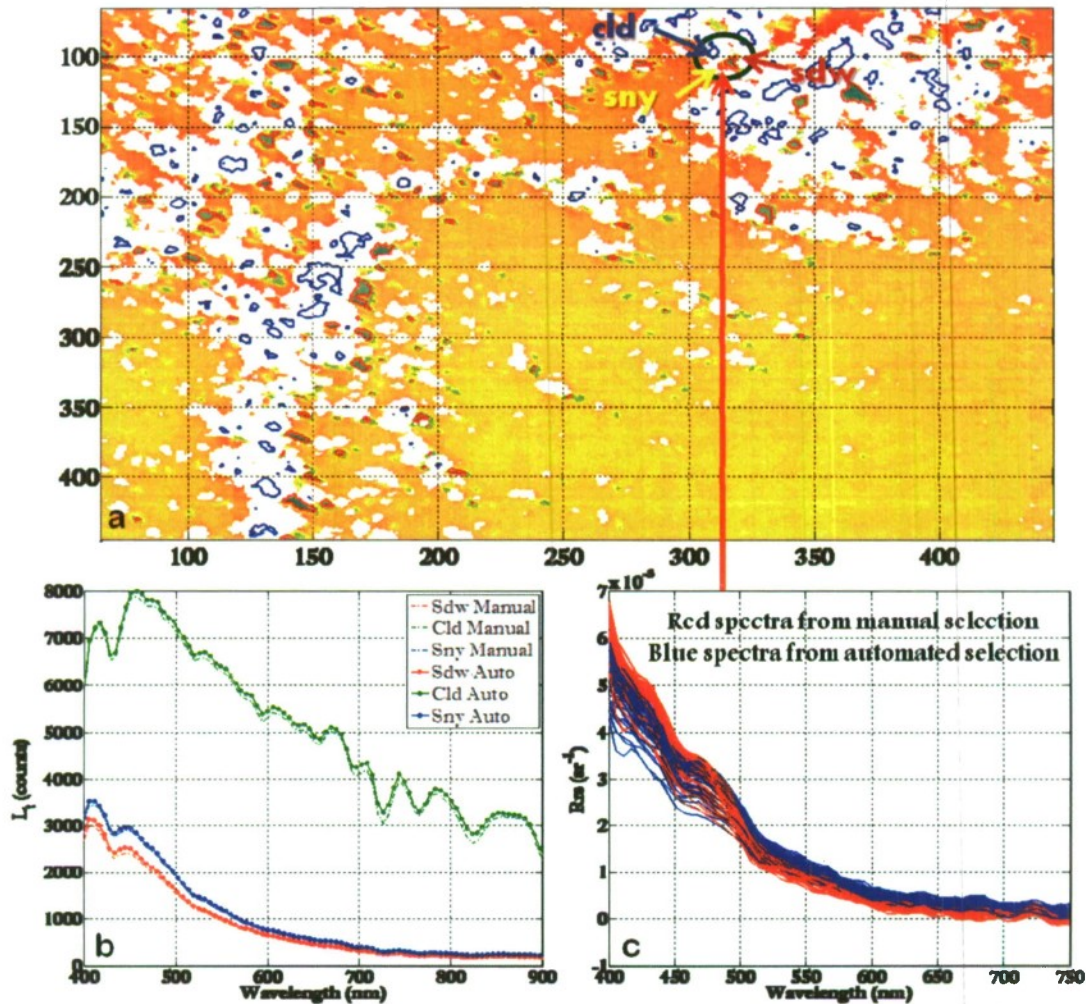
Figure 4. (a) IV image calculated from the HICO image acquired over Samoa Island on October 2, 2010 (image size: 380 × 380 pixels). Clouds are shown in white and the shadows are shown in slightly cooler color compared to the surrounding sunny regions. The blue contours show the thick cloud blobs while the red contours show the thick shadow blobs. (b) The TOA radiance in raw counts of the selected (manually and automatically) from cloud, shadow and sunny pixels ($Lt_{cld}(\lambda)$, $Lt_{sdw}(\lambda)$ and $Lt_{sny}(\lambda)$). (c) The results ($R_{rs}(\lambda)$) of the automatically selected and manually selected pixels taken from the pixels in selected sunny blob.

4. CONCLUSION

Our preliminary results show that the automated procedures of the CSA cloud shadow detection algorithm and the C&S atmospheric correction algorithm works reasonably well on selected HICO images. However, further testing with more images is required to evaluate the overall performance of the automated procedures. The result (remote-sensing reflectance) of the automated and manual C&S atmospheric correction agrees very well suggesting that the automated C&S atmospheric corrections procedure is working. Similarly, the agreement between the true color, IV and the CSA images suggesting that the shadow detection procedure is also working.

ACKNOWLEDGEMENTS

REFERENCES

[1] A. S. Belward and C. R. Valenzuela, "Remote sensing and geographical information system for resource management in developing countries," Kluwer Academic Publishers, Dordrecht/Boston/London, (1991).

[2] P. M. Dare, "Shadow analysis in high-resolution satellite imagery of urban areas," Photogrammetric Engr. & Remote Sens. **71**, 169-177 (2005).

[3] J. J. Simpson and J. R. Stitt, "A procedure for the detection and removal of cloud shadow from AVHRR data over land," IEEE Trans. Geosci. Remote Sens. **36**, 880-897, (1998).

[4] R. Amin, J. Zhou, A. Gilerson, B. Gross, F. Moshary and S. Ahmed, "Novel optical techniques for detecting and classifying toxic dinoflagellate *Karenia brevis* blooms using satellite imagery," Opt. Exp. **17**, 9126-9144 (2009).

[5] R. Amin, A. Gilerson, J. Zhou, B. Gross, F. Moshary and S. Ahmed, "Impacts of atmospheric corrections on algal bloom detection techniques," 89th AMS Annual Meeting, Phoenix, Arizona, January 11-15, (2008).

[6] K. L. Carder, P. Reinersman, R. F. Chen, "AVIRIS calibration using the cloud-shadow method," *Summaries of the Fourth Annual JPL Airborne Geoscience Workshop*, (R. O. Green, ed.) JPL Publication 92-14, **1**, 26-28 (1992).

[7] Z. P. Lee, B. Casey, R. Arnone, A. Weidemann, R. Parsons, M. J. Montes, B. Gao, W. Goode, C. O. Davis, J. Dye, "Water and bottom properties of a coastal environment derived from Hyperion data measured from the EO-1 spacecraft platform," J. Appl. Remote Sens. **1**, 011502 (2007)

[8] P. Reinersman, K. L. Carder, and F. R. Chen, "Satellite-sensor calibration verification with the cloud-shadow method," Appl. Opt. **37**, 5541-5549 (1998).

[9] K. V. Khlopenkov and A. P. Trishchenko,"SPARC: New cloud, snow, and cloud shadow detection scheme for historical 1-km AVHHR data over Canada," J. Atmos. Ocean. Tech. **24**, 322-343 (2007).

[10] S. A. Ackerman, K. I. Strabala, P. Menzel, R. A. Frey, C. C. Moeller, and L. E. Gumley, "Discriminating clear sky from clouds with MODIS," J. Geophys. Res. **103**, 32141-32157 (1998).

[11] J. Cihlar, J. Howarth, "Detection and removal of cloud contamination from AVHRR images," IEEE Trans. Geos. Remote Sens., **32**, 583-589 (1994).

[12] W. B. Rossow, L. C. Garder, "Cloud detection using satellite measurements of infrared and visible radiances for ISCCP." J. Clima. **6**, 2341-2369 (1993).

[13] P. Y. Chen, R. Srinivasan, G. Fedosejevs, B. Narasimhan, "An automated cloud detection method for daily NOAA-14 AVHRR data for Texas, USA." Int. J. Remote Sens. **23**, 2939-2950 (2002).

[14] B. Wang, A. Ono, "Automated detection and removal of clouds and their shadows from Landsat TM images," IEICE Trans. Inf. & Syst., **E82-D**, 453-460, (1999).

[15] J. J. Simpson, Z. Jin, and J. R. Stitt, "Cloud shadow detection under arbitrary viewing and illumination conditions," IEEE Trans. Geosci. Remote Sens. **38**, 972-976 (2000).

[16] H. R. Gordon, and M. Wang, "Retrieval of water-leaving radiance and aerosol optical thickness over the oceans with SeaWiFS: a preliminary algorithm," Appl. Opt. **33**, 443-452 (1994)

[17] R. P. Stumpf, R. A. Arnone, R. W. Gould, P. M. Martinolich, V. Ransibrahmanakul, "A partially coupled ocean-atmosphere model for retrieval of water-leaving radiance from SeaWiFS in coastal waters," *SeaWiFS postlaunch technical report series, Vol. 22*, S. B. Hooker and E. R. Firestone, Eds., *NASA/TM-2003-206892, (2003)*

[18] M. Wang, and W. Shi, "Estimation of ocean contribution at MODIS near infrared wavelengths along the east coast of the U.S.: two case studies," Geophys. Res. Lett. **32**, L13606, doi: 10.1029/2005GL022917, (2005)

[19] R. Amin, R. Gould, W. Hou, R. Arnone, Z. Lee, " Optical algorithm for cloud shadow detection over water," Appl. Opt. (submitted)

[20] R. Richter and A. Muller, "De-shadowing of satellite/airborne imagery," Int. J. Remote Sens., **26**, 3137-3148 (2005).

[21] Z. P. Lee, K. L. Carder, C. D. Mobley, R. G. Steward, and J. S. Patch, "Hyperspectral remote sensing for shallow waters. 1. A semianalytical model," Appl. Opt. **37**, 6329-6338 (1998)

[22] J. T. O. Kirk, "Volume scattering function, average cosines, and the underwater light field," Limnol. Oceanogr. **36**, 455-467 (1991)

[23] A. Morel and B. Gentili, "Diffuse reflectance of oceanic waters (2): Bi-directional aspects," Appl. Opt. **32**, 6864-6879 (1993)

[24] Z. P. Lee, K. L. Carder, and K. P. Du, "Effects of molecular and particle scattering on model parameters for remote-sensing reflectance, "Appl. Opt. **43**, 4957-4964 (2004)

[25] W. W. Gregg and K. L. Carder, "A simple spectral solar irradiance model for cloudless maritime atmospheres," Limnol., Oceanogr, **35**, 1657-1675 (1990)

[26] H. R. Gordon and D. K. Clark, "Clear water radiances for atmospheric correction of coastal zone color scanner imagery," Appl. Opt. **20**, 4175-4180 (1981)

[27] J. L. Mueller, C. Davis, R. Arnone, R. Frouin, K. L. Carder, Z. P. Lee, R. G. Steward, S. Hooker, C. D. Mobley, and S. McLean, " Above-water radiance and remote sensing reflectance measurement and analysis protocols," *in Ocean Optics Protocols for Satellite Ocean Color Sensor Validation*, **Revision 3**, J. L. Mueller and G. S. Fargion, Eds., *NASA/TM-2002-210004*, 171-182 (2002)